Dead Beat Predictive DPC based Battery Charging System Using Dynamic DC-link Reference

Abinash Rath
Department of Electrical Engineering
NIT, Rourkela
E-mail- abinash_rath@nitrkl.ac.in

Gopalakrishna Srungavarapu
Department of Electrical Engineering
NIT, Rourkela
E-mail-gopal@nitrkl.ac.in

***Abstract*— The usage of the Li-ion batteries in different applications like UPS, electric vehicles (EVs), and other energy storage devices are growing day by day. A delicate charging system is needed for long battery life which should operate at high power quality. Because of its fast dynamic response, the Direct Power Control (DPC) is an excellent alternative to the ac-dc converter in grid-connected charging systems. Traditional DPC-based charging systems operate in two stages, with a dc-dc buck converter accurately managing the charging voltage to ensure rapid charging. This work presents a dead beat predictive control strategy that eradicates the dc-dc converter from the conventional system by using a dynamical dc-link voltage reference in the ac-dc converter itself. As the system's hardware requirements are lowered, the overall size, weight, and cost are reduced. MATLAB simulation models have been built for the proposed method and it is further extended to real-time simulation in the RT-LAB environment to ensure that the proposed strategy is feasible.**

Keywords*— *Direct power control (DPC), EV Battery Charging, Dead Beat Predictive DPC (DB-DPC), Dynamic dc-link reference, CC/CV charging, Real-time Simulation

I. INTRODUCTION

The environmental impact and efficient features of electric vehicles are making them popular all over the world. Apart from EVs, household inverters, UPS, and many industrial applications too require batteries. So designing of the efficient charging system is the need of the hour. When the battery is grid-connected through a bidirectional converter, the power can flow in both directions. When the grid power is used to charge the battery, the mode of operation is called as the grid to vehicle (G2V), and conversely, when the power flow reverses, it is known as the vehicle to grid (V2G) operation [1], [2].

The Li-ion (Lithium-ion) batteries present features like high power density (twice of Ni-Cd), low self-discharging, and ability to produce high power etc. for which they are well-received in many applications. On the counter side, the battery life is sensitive towards frequent change in current directions or taking charge from a high ripple current. Hence a carefully designed charging system is essential for Li-ion batteries to have reasonably good battery life [3].

The use of DPC for ac-dc converter control has provided additional benefits such as faster dynamic response and the eradication of the internal current control loop [4]. Integrating SVM for constant switching frequency operation [5], virtual flux approach to remove grid-side voltage sensors [6], dynamic tables based on demand magnitude [7], [8], duty ratio control [9], etc. have made the DPC an even better tool for ac-dc converter control. Because of its control accuracy, the model predictive control (MPC) has been regarded as one of the best DPC techniques [10], [11]. It is more versatile than other predictive control schemes, such as dead beat predictive DPC [12], since it can handle additional nonlinear constraints. Several alterations in the cost function have been reported as extra features in the control operation, such as reduced switching loss, DC link voltage ripple, coupling between active and reactive power control, and so on [13]. The MPC, on the other hand, necessitates a greater degree of computing efficiency from the executing processor [12].

PI controllers and voltage oriented control have been used to control chargers in the past. Because of their fast dynamic performance, DPC-based converters have recently been employed in these EV charging stations. In the G2V mode of operation, the literature presents an MPC-based converter feeding a bidirectional dc-dc converter that finally connects the battery to the grid [1]. To enhance the power handling potential, a deadbeat predictive DPC controlled active front-end rectifier is utilized to charge the battery in, followed by an interleaved buck converter [3]. To link the battery to the DC side of the grid-connected rectifier, all DPC-based EV charging techniques documented in the literature employ a dc-dc converter in the intermediate stage.

The aim of this research work is to develop a grid-connected charging system using only an ac-dc converter that draws power at high power quality indices. Hence the dc-dc converter forming stage II of the conventional DPC-based charging system can be eliminated entirely to achieve less hardware requirement for physical implementation. In contrast to the traditional method, the proposed method does not require the deployment of a dc-dc converter to govern the charging voltage. Instead of employing dynamic referring with the dc-dc converter, the DPC approach uses a dynamic DC-link reference in the outer control loop. This dc-link voltage is regulated to keep the charging current via the battery constant. The abolition of this buck converter decreases the design complexity as well as the overall hardware requirements, lowering the total setup cost.

II. CONVENTIONAL DPC BASED CHARGING SYSTEM

Fig. 1 shows the control organization of traditional DPC-based EV charging in a blocks diagram. The charging system in this method consists of two independent phases of power converters. The MP-DPC method is used in the first of two phases to convert three-phase ac to a fixed dc voltage. Using a bidirectional dc-dc converter controlled by a PWM block, this fixed dc is converted to a variable dc once more. Through the line inductance (L), the grid feeds the IGBT-based converter module. Clarke's transformation is used to convert the estimated grid side voltage and currents from three phase to two phase on a given reference frame (α-β). The alpha and beta components of the grid voltages and currents are used to estimate the instantaneous active and reactive power using the instantaneous power theory. To identify the best switching combination, a cost function containing the errors in active and reactive power is minimized.

| //$31.00 ©10.1109/NPEC52100.2021.9672500

978-1-6654-1023-6/21/$31.00 ©2021 IEEE

The bidirectional dc-dc converter that feeds the battery at the desired charging current is controlled using dynamic reference in the second stage. For this, the battery current is measured and compared to the target value on a regular basis. A PWM block assesses the duty ratio of the gate pulse based on the obtained inaccuracy in order to track the target charging current [1].

The use of an interleaved multi-leg buck converter has been proposed to boost the power handling capability even more. The control of this type of multi-leg with '*m*' number of legs necessitates the use of '*m*' carrier waves. A phase difference of '*2/m*' is used to generate the carrier waves. With this the corresponding frequency for change in the current magnitude increases by '*m*' times and the ripple is minimized too [3].

However, it necessitates the addition of another '*m*' number of additional switching devices and inductors. The total procedure is complicated due to the introduction of various carrier signals and their management.

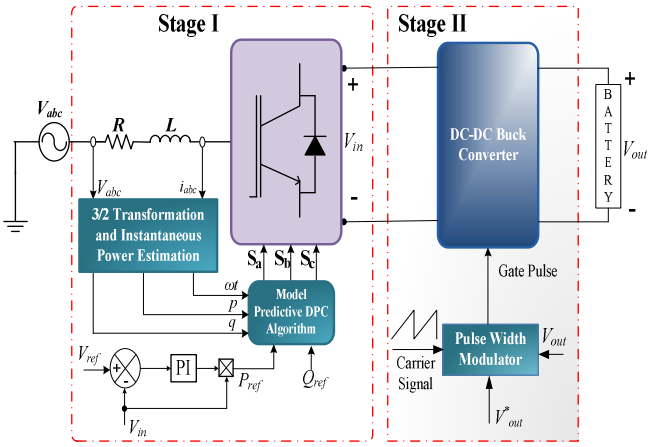

Fig. 1. A schematic representation of traditional DPC based battery charger

III. Proposed Charging System

Here an effectual and uncomplicated modification is presented in the control structure, which doesn't require the DC-DC converter following the ac-dc converter connected to the grid. Dead beat predictive DPC [12] is chosen as the control method of the rectifier as it has more accurate in the control of active and reactive power than the conventional DPC [4]. The constant switching frequency also enables an easier designing process for the filter components.

A. Dead Beat Predictive Control

The dead beat predictive DPC aims at finding the rectifier end average Voltage vector, which is capable of meeting the active power and reactive power demand. This control algorithm takes the instantaneous active power, reactive power, and their references as input and produces the stationary axis components of the rectifier end voltage, which would lead to achieving the control objectives. Using the space vector modulation technique, the PWM signal for each of the switching devices is generated [12].

From the *pq* theory, the instantaneous active and reactive powers can be expressed in terms of the stationary reference frame components of the grid voltage ($V_{\alpha\beta}$) and current ($i_{\alpha\beta}$) as shown in (1).

$$\begin{bmatrix} p \\ q \end{bmatrix} = \begin{bmatrix} V_\alpha & V_\beta \\ V_\beta & -V_\alpha \end{bmatrix} \begin{bmatrix} i_\alpha \\ i_\beta \end{bmatrix} \tag{1}$$

The incremental change in '*p*' and '*q*' between two consecutive samples considering the sampling interval to be very small can be given by the expression shown in (2). Here, the change in the grid voltage vectors in one sampling period is neglected as it is very small [12].

$$\begin{bmatrix} p(n+1)-p(n) \\ q(n+1)-q(n) \end{bmatrix} = \begin{bmatrix} V_\alpha & V_\beta \\ V_\beta & -V_\alpha \end{bmatrix} \begin{bmatrix} i_\alpha(n+1)-i_\alpha(n) \\ i_\beta(n+1)-i_\beta(n) \end{bmatrix} \tag{2}$$

Using the voltage balance relation on the ac side of the converter shown in fig. 3, the grid voltage and the rectifier end voltage can be related as (3).

$$V_{\alpha\beta} - Ri_{\alpha\beta} - L\frac{d}{dt}i_{\alpha\beta} - v_{\alpha\beta} = 0 \tag{3}$$

From (3), the expressions for the time differential of the line current can be expressed as shown in (4).

$$\frac{d}{dt}\begin{bmatrix} i_\alpha \\ i_\beta \end{bmatrix} = \frac{1}{L}\begin{bmatrix} V_\alpha \\ V_\beta \end{bmatrix} - \frac{1}{L}\begin{bmatrix} v_\alpha \\ v_\beta \end{bmatrix} - \frac{R}{L}\begin{bmatrix} i_\alpha \\ i_\beta \end{bmatrix} \tag{4}$$

Neglecting the effect of the ESR and using Euler's approximation to find the difference between the current values at the k^{th} instant and the $(k+1)^{th}$ instant can be obtained as shown in (5).

$$\begin{bmatrix} i_\alpha(n+1)-i_\alpha(n) \\ i_\beta(n+1)-i_\beta(n) \end{bmatrix} = \frac{T_s}{L}\left(\begin{bmatrix} V_\alpha(n) \\ V_\beta(n) \end{bmatrix} - \begin{bmatrix} v_\alpha(n) \\ v_\beta(n) \end{bmatrix}\right) \tag{5}$$

Replacing (5), in (2)

$$\begin{bmatrix} p(n+1)-p(n) \\ q(n+1)-q(n) \end{bmatrix} = \begin{bmatrix} V_\alpha(n) & V_\beta(n) \\ V_\beta(n) & -V_\alpha(n) \end{bmatrix} \times \frac{T_s}{L}\left(\begin{bmatrix} V_\alpha(n) \\ V_\beta(n) \end{bmatrix} - \begin{bmatrix} v_\alpha(n) \\ v_\beta(n) \end{bmatrix}\right) \tag{6}$$

Rearranging (6), the expressions of the rectifier end voltage can be obtained as shown in (7), which is fed to the SVM block that finally produces the PWM signal at a constant switching frequency.

$$\begin{bmatrix} v_\alpha(n) \\ v_\beta(n) \end{bmatrix} = \begin{bmatrix} V_\alpha(n) \\ V_\beta(n) \end{bmatrix} - \frac{L}{T_s\left|V_{\alpha\beta}\right|}\begin{bmatrix} V_\alpha(n) & V_\beta(n) \\ V_\beta(n) & -V_\alpha(n) \end{bmatrix} \times \begin{bmatrix} p(n+1)-p(n) \\ q(n+1)-q(n) \end{bmatrix} \tag{7}$$

As the aim of this DPC method is to maintain the consumed powers at their desired level, *p(n+1)* and *q(n+1)* in (7) correspond to the respective reference values in the control structure. To compensate for the adverse effects of the control delay, the predicted values of '*p*' and '*q*' are used. The final

expression for the stationary axis components of the rectifier end voltage can be obtained as shown in (8).

$$\begin{bmatrix} v_\alpha(n) \\ v_\beta(n) \end{bmatrix} = \begin{bmatrix} V_\alpha(n) \\ V_\beta(n) \end{bmatrix} - \frac{L}{T_s \left| V_{\alpha\beta} \right|} \begin{bmatrix} V_\alpha(n) & V_\beta(n) \\ V_\beta(n) & -V_\alpha(n) \end{bmatrix} \times \begin{bmatrix} P_{ref}(n) - P_{ref}(n-1) - e_p(n) \\ e_q(n) \end{bmatrix} \quad (8)$$

Where $e_p(n)$ and $e_q(n)$ are the errors in the active and reactive power control.

The space vector modulator block generates the required PWM signal for the switches in the power converter at the constant switching frequency.

B. Design of the dynamic dc-link reference

Instead of controlling the DC link voltage directly, the charging current drawn from the dc side of the converter is controlled in this proposed method. Figure 2 depicts the entire control mechanism.

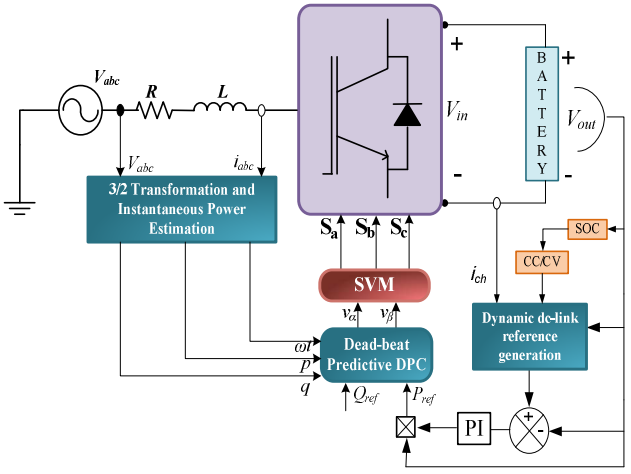

Fig. 2. Schematic representation of the proposed method

The required change in the charging current is reflected in the change in the dc-link voltage. To achieve fast charging of the battery, the reference charging current is set to its nominal value, which in this case is 6 A. The produced error in the measured battery current (i_{ch}) is sent to a PI controller after 'i_{ch}' is compared with the reference charging current (i^*_{ch}). The deviation in the charging current 'Δi_{ch}' can be expressed mathematically as (9).

$$\Delta i_{ch} = i^*_{ch} - i_{ch} \quad (9)$$

The battery charging current is regulated by the PI controller around its set point. The error in the dc-link voltage reference (ΔV_{ref}) which is the PI controller's output, is added to the nominal dc-link voltage reference (V'_{ref}) to form the dynamic dc-link reference (V^*_{ref}). Equations (9) and (10) illustrate the mathematical expressions for 'V'_{ref}' and 'V^*_{ref}', respectively.

$$\Delta V_{ref} = (k_p + \frac{k_i}{s})\Delta i_{ch} \quad (9)$$

$$V^*_{ref} = V'_{ref} + \Delta V_{ref} \quad (10)$$

The final expression for the dynamic dc-link reference can be derived by replacing the expression of 'V_{ref}' in (10) with the expression obtained from (9).

$$V^*_{ref} = V'_{ref} + (k_p + \frac{k_i}{s})\Delta i_{ch} \quad (11)$$

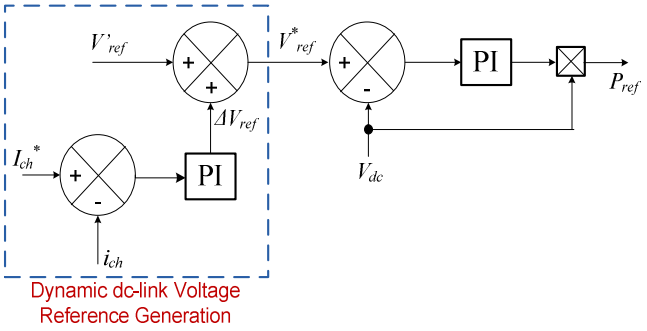

Fig. 3. Dynamic dc-link reference generation

The entire process of dynamic reference generation is illustrated in fig. 3 as a block diagram.

C. CC/CV Charging

The constant current and constant voltage (CC/CV) charging, which is a well-established method for Li-ion batteries, is employed in this system. The mode of charging is decided by the state of charge (SOC) of the battery. The SOC is measured from the battery voltage as per the model presented in [14].

A predetermined set value of the charging current is forced through the battery to reduce the charging time in CC mode. This set value of the charging current is kept around the nominal battery current. In CV mode, a constant charging voltage equal to the maximum attainable no-load voltage of the battery is fed to the battery. When the SOC reaches 90%, the charging mode is switched from CC mode to CV mode. In CV mode, with the rising SOC of the battery, the charging current keeps decreasing. When the charging current reaches a value that is 10% of the nominal battery current, the charging process is aborted, considering the battery is fully charged. Deployment of this CC/CV charging is essential for minimizing the charging time without doing any harm to the battery life.

D. Real-Time Simulation

In any digital simulation, the computer solves the mathematical functions and equations described in the system model to produce some output. The time taken by the digital computer to evaluate the system model to produce the outcome may be less or more than the simulation time step. This is where the real-time simulation is different from the offline digital simulation as the simulation time runs at the same speed as the real physical clock [15]. In an offline simulation, the execution time depends on the complexity of the system model as the controller in each step waits till the result is available to resume the next step execution. Whereas in the case of the real-time simulation, the controller only waits till the completion of the simulation step time. In this case, whether the final output of the mathematical process is reached or not remains irrelevant to begin the next step [16]. If the system model can not be evaluated within the stipulated step time, an erroneous output is resulted, which is generally termed as overrun. So when a system model operates without

overrun in a real-time digital simulator, it indicates that the processor is able to complete all necessary computations, including the IO processing. It certifies that the given model will not produce an overrun when it is subjected to physical implementation. But this concept of overrun doesn't come up in the case of offline simulation, which may restrict the operation when the model is implemented practically.

Fig. 4 shows a picture of the real-time simulation environment where the real-time simulator can be seen which is connected to the host PC via LAN cable. The MATLAB simulation model is built in the host PC, but it is run on the RT-LAB environment which is equipped with the OP5142 real-time simulator. A quad-core Xeon processor by Intel processes the system model with the simulation time-synchronized to the real-world clock.

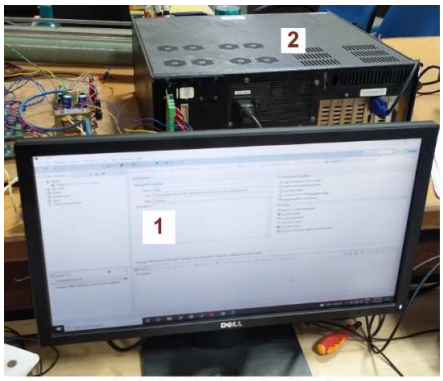

1. Host PC, 2. RT-Lab Real-time Simulator

Fig. 4. RT-Lab Setup fror real-time simulation

IV. Result Analysis

The proposed method's feasibility and performance are evaluated in the MATLAB/Simulink environment and RT-LAB environment. The obtained results from the real-time simulation are saved from the consol of the RT-LAB environment as a MATLAB file with .mat extension. Here a Li-ion battery with a nominal voltage of 120 V is used, having a current rating of 6.33 A at the nominal voltage. The system parameters used in this model are given in the Appendix section.

Fig. 5 depicts some key performance factors during the proposed battery charging system's steady-state operation. The waveforms of lowered phase voltage by a factor of two and the phase current of phase '*a*' can be seen in fig. 5 (a). The zero crossings of both waveforms coincide, indicating a high displacement power factor. The current waveforms of all three phases are shown in Fig. 5 (b). The dynamically controlled dc-link voltage of the converter is shown in Fig. 5 (c), and it is constantly changing in order to generate the necessary charging current. The SOC of the battery is shown in Fig. 5 (d), and it appears to be increasing as the battery receives active power. The waveforms of the instantaneous active power (p) and the reactive power (q) are shown in fig. 5 (e). The charging system consumes an average of 844 W of active power. The active power and reactive power have ripple content of 28.48 W and 21.88 Var, respectively. The standard deviations of the different samples obtained over 1s during the steady-state operation are used to calculate the ripple contents. The battery current waveform is shown in Fig. 5 (f). It appears to oscillate about the battery current reference of -6A. The negative sign signifies that the battery is receiving power. The line current spectrum is analyzed using the FFT analysis to determine the grid power quality. The exact shape of the current on which the FFT is applied is depicted in fig. 6 (a). Figure 6 (b) depicts the obtained spectrum of line current in which 3.08% of total harmonic distortion (THD) was discovered.

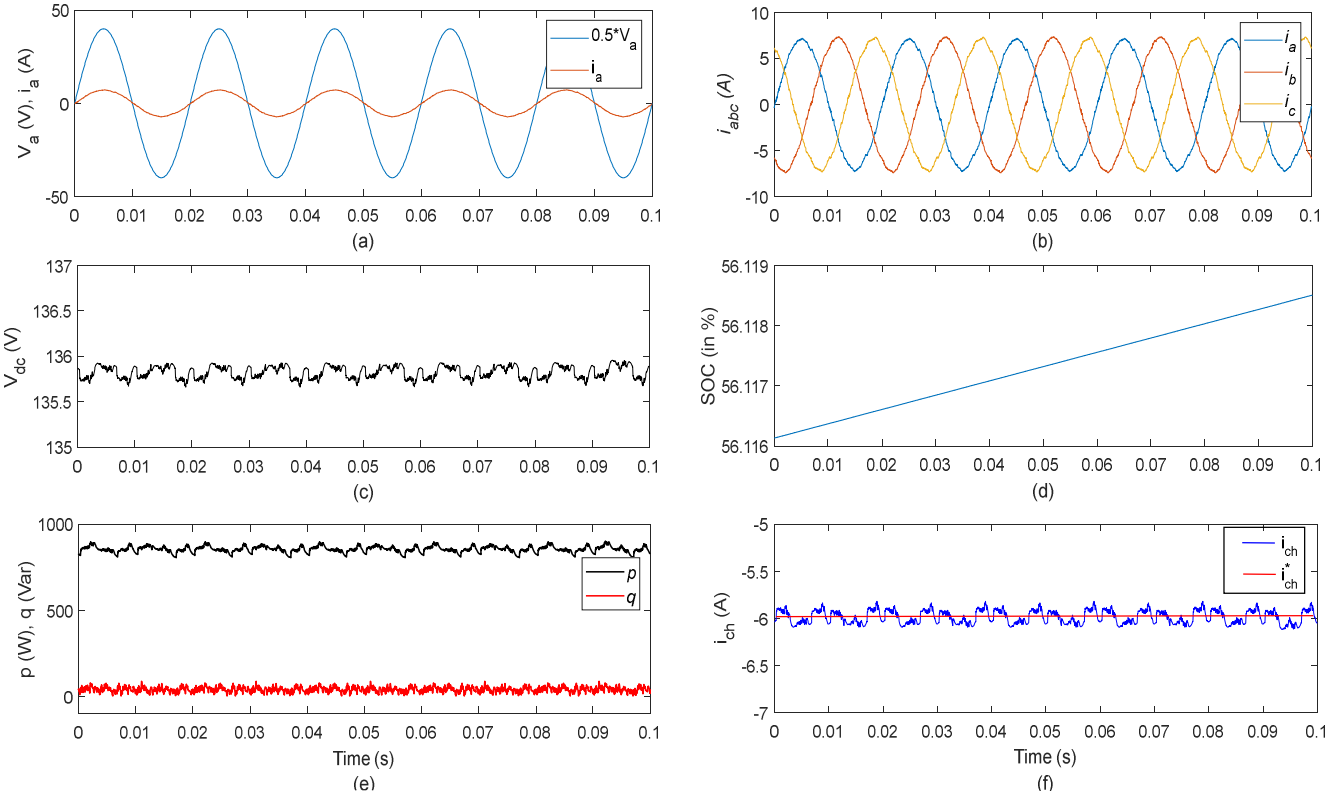

Fig. 5. Steady state waveforms of (a) $0.5V_a$ and i_a (b) line current (c) output dc voltage (d) SOC of battery (e) instantaneous active and reactive power (f) charging current

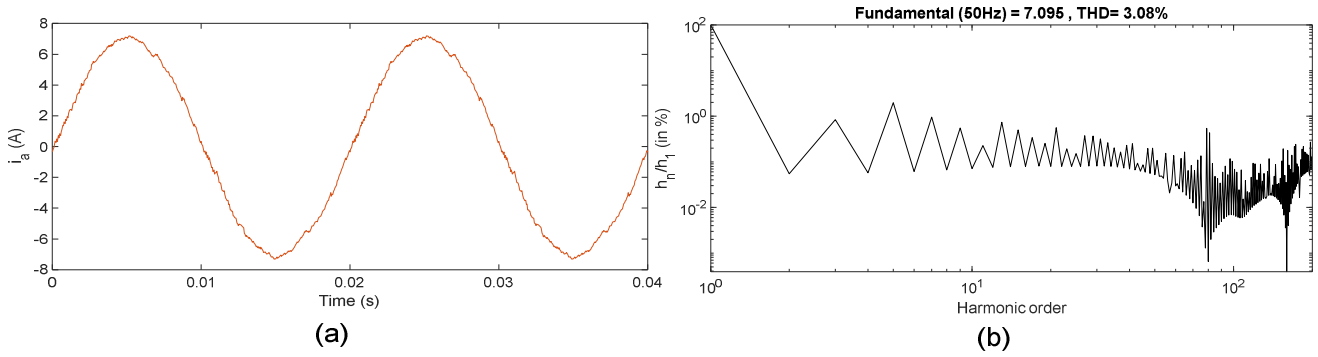

Fig. 6. Harmonic content analysis of line current (a) Line Current waveform (b) Line current spectrum

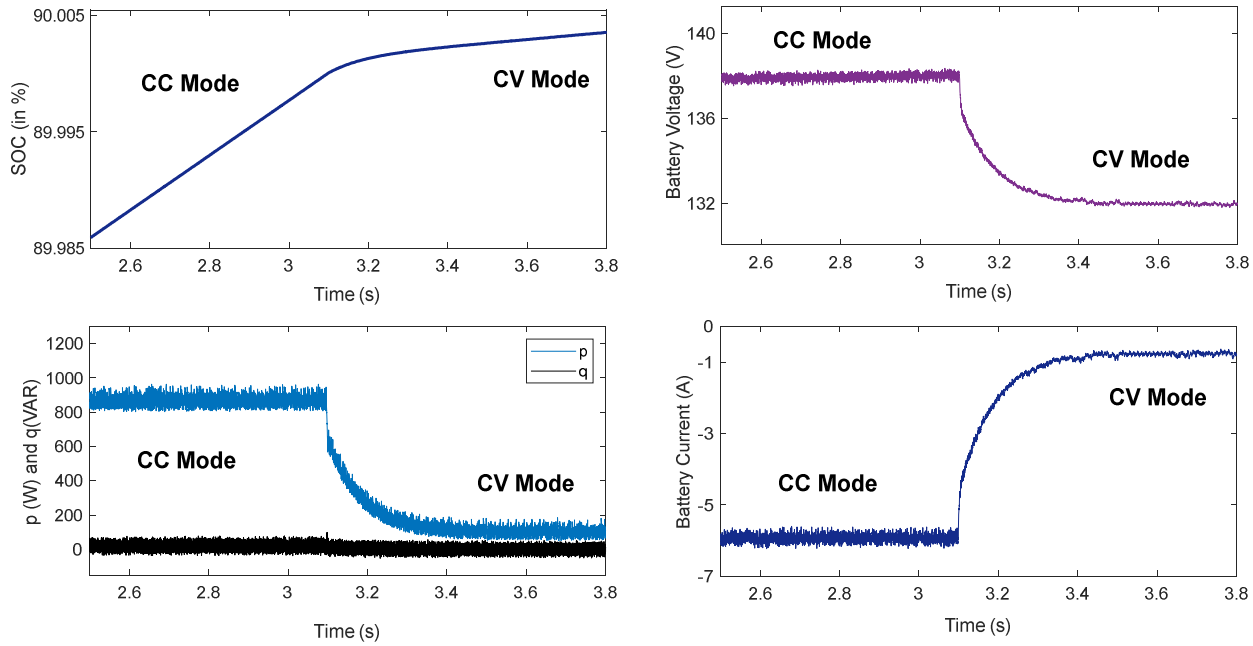

Fig. 7. The transition of CC mode to CV mode

Some physical parameters of the battery charging system during the transitional period of CC mode to CV mode of charging is shown in fig. 7. When the SOC of the Li-ion battery reaches 90%, the mode of charging is altered from CC to CV. It can be observed from the waveforms of SOC which has a reduced slope on the CV mode, the charging current, and the consumed active power, which are far too less in the CV mode, that the rate of charging has been reduced in this mode of charging as compared to the CC mode. The charging voltage is now reduced to the maximum attainable battery voltage in the no-load condition. The oscillation of the instantaneous reactive power about 0 Var indicates that the converter still operates at a high power factor. The charging current in the CV mode reduces to -1 A from its magnitude of -6 A in the CC mode. With the rising SOC, this charging current will go on decreasing, and finally, the battery charging will be terminated when it reaches 0.6 A, which is 10% of the CC mode charging current.

Performance indicators such as line current THD, ripple content of instantaneous powers, and charging current are reported in Table 1 for a comparative examination. Because the performance indices for both approaches are similar, it can be concluded that the proposed method, which does not use a dc-dc converter, is still as effective as the conventional method. As the future scope of this work includes the physical implementation of the system, the circuit parameters in the simulation work are chosen considering the rating of the available instruments in the laboratory. The system can be easily redesigned with any other supply voltage.

TABLE I. COMPARATIVE ANALYSIS OF THE PERFORMANCE INDICES

Performance Index	Conventional Method [1]	Proposed Method
Line Current THD	3.79%	3.08%
Active power ripple	28.07 W	26.48 W
Reactive power ripple	22.64 Var	21.88 Var
Battery current ripple	0.088 A	0.070 A

V. CONCLUSION

Here in this research work, a grid-connected battery charging system employs the dead beat predictive DPC method for the control of the ac-dc converter. It successfully eliminates the use of dc-dc converter in stage II by using a dynamic dc-link referencing in the ac-dc converter itself. The performance parameters obtained from the results section confirm that the proposed method provides good control on the charging current without degrading the grid power quality. The constant switching frequency operation because of the SVM also makes the filter design an easier task. Low values of the ripple contents in the instantaneous active and reactive powers and the line current THD signifies accuracy in control

along with reasonably good power quality on the grid side (as THD is less than the standard value of 5%). Validation of the proposed method in a real-time environment confirms it's feasibility in a practical system as well.

APPENDIX

Symbols	Description	System Parameters
U_{abc}	The three-phase voltages	80 V
R_s	ESR of inductance	0.2 Ω
L	Line filter inductance	10 mH
T_s	Sampling time period	50 ms
C	DC bus capacitance	2000 μF

REFERENCES

[1] T. He, M. Wu, D. D. C. Lu, R. P. Aguilera, J. Zhang, and J. Zhu, "Designed Dynamic Reference with Model Predictive Control for Bidirectional EV Chargers," *IEEE Access*, vol. 7, pp. 129362–129375, 2019, doi: 10.1109/ACCESS.2019.2940214.

[2] P. Wang, Y. Bi, F. Gao, T. Song, and Y. Zhang, "An Improved Deadbeat Control Method for Single-Phase PWM Rectifiers in Charging System for EVs," *IEEE Trans. Veh. Technol.*, vol. 68, no. 10, pp. 9672–9681, 2019, doi: 10.1109/TVT.2019.2937653.

[3] H. W. Choi, S. M. Kim, J. Kim, Y. Cho, and K. B. Lee, "Deadbeat predictive direct power control of interleaved buck converter-based fast battery chargers for electric vehicles," *J. Power Electron.*, vol. 20, no. 5, pp. 1162–1171, 2020, doi: 10.1007/s43236-020-00106-7.

[4] T. Noguchi, H. Tomiki, S. Kondo, and I. Takahashi, "Direct power control of PWM converter without power-source voltage sensors," *IEEE Trans. Ind. Appl.*, vol. 34, no. 3, pp. 473–479, 1998, doi: 10.1109/28.673716.

[5] M. Malinowski, M. Jasiński, and M. P. Kazmierkowski, "Simple direct power control of three-phase PWM rectifier using space-vector modulation (DPC-SVM)," *IEEE Trans. Ind. Electron.*, vol. 51, no. 2, pp. 447–454, 2004, doi: 10.1109/TIE.2004.825278.

[6] A. M. Razali, M. A. Rahman, G. George, and N. A. Rahim, "Analysis and Design of New Switching Lookup Table for Virtual Flux Direct Power Control of Grid-Connected Three-Phase PWM AC-DC Converter," *IEEE Trans. Ind. Appl.*, vol. 51, no. 2, pp. 1189–1200, 2015, doi: 10.1109/TIA.2014.2344503.

[7] J. G. Norniella *et al.*, "Multiple switching tables direct power control of active front-end rectifiers," *IET Power Electron.*, vol. 7, no. 6, pp. 1578–1589, 2014, doi: 10.1049/iet-pel.2013.0492.

[8] A. Rath, A. Kumar, G. Srungavarapu, and M. Pattnaik, "Power quality improvement using 18 sector algorithm based direct power control," *Int. Trans. Electr. Energy Syst.*, no. April 2020, pp. 1–17, 2021, doi: 10.1002/2050-7038.12784.

[9] Y. Zhang, Z. Li, Y. Zhang, W. Xie, Z. Piao, and C. Hu, "Performance improvement of direct power control of pwm rectifier with simple calculation," *IEEE Trans. Power Electron.*, vol. 28, no. 7, pp. 3428–3437, 2013, doi: 10.1109/TPEL.2012.2222050.

[10] P. Cortés, J. Rodríguez, P. Antoniewicz, and M. Kazmierkowski, "Direct power control of an AFE using predictive control," *IEEE Trans. Power Electron.*, vol. 23, no. 5, pp. 2516–2523, 2008, doi: 10.1109/TPEL.2008.2002065.

[11] A. Rath and G. Srungavarapu, "New Model Predictive Algorithm DPC based Shunt Active Power Filters (SAPFs)," *ICPEE 2021 - 2021 1st Int. Conf. Power Electron. Energy*, no. 3, pp. 48–53, 2021, doi: 10.1109/ICPEE50452.2021.9358550.

[12] A. Bouafia, J. P. Gaubert, and F. Krim, "Predictive direct power control of three-phase pulsewidth modulation (PWM) rectifier using space-vector modulation (SVM)," *IEEE Trans. Power Electron.*, vol. 25, no. 1, pp. 228–236, 2010, doi: 10.1109/TPEL.2009.2028731.

[13] D. K. Choi and K. B. Lee, "Dynamic performance improvement of AC/DC converter using model predictive direct power control with finite control set," *IEEE Trans. Ind. Electron.*, vol. 62, no. 2, pp. 757–767, 2015, doi: 10.1109/TIE.2014.2352214.

[14] W. Shen, T. T. Vo, and A. Kapoor, "Charging algorithms of lithium-ion batteries: An overview," *Proc. 2012 7th IEEE Conf. Ind. Electron. Appl. ICIEA 2012*, pp. 1567–1572, 2012, doi: 10.1109/ICIEA.2012.6360973.

[15] F. Li *et al.*, "Review of Real-time Simulation of Power Electronics," *J. Mod. Power Syst. Clean Energy*, vol. 8, no. 4, pp. 796–808, 2020, doi: 10.35833/MPCE.2018.000560.

[16] S. Vazquez *et al.*, "Model predictive control: A review of its applications in power electronics," *IEEE Ind. Electron. Mag.*, vol. 8, no. 1, pp. 16–31, 2014, doi: 10.1109/MIE.2013.2290138.